

THE KUIPER BELT AND OLBERS PARADOX

SCOTT J. KENYON

Smithsonian Astrophysical Observatory, 60 Garden Street, Cambridge, MA 02138

skenyon@cfa.harvard.edu

AND

ROGIER A. WINDHORST

Dept of Physics & Astronomy, Arizona State University, Box 871504, Tempe, AZ 85287-1504

Rogier.Windhorst@asu.edu

Re-submitted to the Astrophysical Journal Letters, 5 October 2000

ABSTRACT

We investigate the constraints that Olbers Paradox, applied to the Zodiacal Background as measured from space, sets on outer solar system objects. If extended to very faint limits, $R \sim 40$ –50 mag, the steep optical number counts of Kuiper Belt objects (KBOs) at $R \lesssim 26$ imply an infinitely bright night sky. Small KBOs with radii of $r \sim 1 \mu\text{m}$ to $r \sim 1 \text{ km}$ must have a size distribution $n(r) \propto r^{-a}$, with $a \sim 3.4$ or smaller to satisfy the known limits on the sky-surface brightness at optical and far-infrared wavelengths. Improved limits on the measured KBO surface brightness can yield direct estimates of the albedo, temperature, and size distribution for small KBOs in the outer solar system.

Subject headings: Kuiper Belt – solar system: formation

1. INTRODUCTION

The darkness of the night sky – Olbers Paradox – is one of astronomy’s great mysteries. The conclusion that an infinite universe full of stars and galaxies produces an infinitely bright sky is over four hundred years old. The resolution of the Paradox, an expanding and infinite universe with a finite age, is now a central tenet of Big Bang Cosmology, where galaxy counts and the limiting sky background constrain the evolution of galaxies and the curvature of the universe (e.g., Driver *et al.* 1995, 1996, 1998; Odewahn *et al.* 1996). Here we show that local radiation sources, including the Kuiper Belt in our solar system, can also appear to violate Olbers Paradox. Current limits on the sky background set interesting constraints on the mass and size distributions of Kuiper Belt objects (KBOs).

Recent observations have detected many small icy bodies in our solar system outside the orbit of Neptune (Luu & Jewitt 1998). These KBOs consist of three dynamical classes: (1) *classical* KBOs with roughly circular orbits and semimajor axes of 41–47 AU, (2) *resonant* KBOs, also known as Plutinos, in orbital resonance with Neptune (Jewitt, Luu, & Chen 1996), and (3) *scattered* KBOs with eccentric orbits, $e \sim 0.5$, and perihelion distances of 30–38 AU (Luu *et al.* 1997). For an adopted optical albedo, $\omega \approx 0.04$, KBOs with red magnitudes, $R \approx 20$ –26 mag, have radii of 50–500 km (Luu & Jewitt 1998).

All optical measurements of individual KBOs are consistent with a simple function for the number counts:

$$\log N(R) = \alpha(R - R_0), \quad (1)$$

where N is the cumulative number of KBOs per square degree.¹ Recent analyses indicate $\alpha = 0.5$ –0.75 and $R_0 = 23.2$ –23.5 mag in the Kron-Cousins photometric system (Gladman *et al.* 1998; Jewitt, Luu, & Trujillo 1998; Chi-

ang & Brown 1999). These results imply a differential size distribution, $n(r) \propto r^{-a}$, where $a = 3.5$ –4.5 (e.g., Luu & Jewitt 1998). The total mass in large KBOs with radii 50–500 km is ~ 0.1 –0.2 M_{\oplus} for the classical and resonant KBOs (Jewitt *et al.* 1998; Luu & Jewitt 1998) and $\sim 0.05 M_{\oplus}$ for the scattered KBOs (Trujillo *et al.* 2000). Coagulation models which form large KBOs from mergers of much smaller objects naturally produce size distributions, $n(r) \propto r^{-4}$, and total masses of large KBOs consistent with the R-band observations (Kenyon & Luu 1999a,b).

Fits to the optical counts of KBOs can conflict with measurements of the known, finite sky brightness. Windhorst, Mathis, & Keel (1992) and Windhorst *et al.* (1994, 1998) quote on-orbit surface brightness measurements with the Hubble Space Telescope (HST) Wide Field/Planetary Camera 1 (WF/PC-1) and Wide Field Planetary Camera 2 (WFPC2) at ecliptic latitude $\approx 70^\circ$ for V, $\mu_V \approx 23.2 \text{ mag arcsec}^{-2}$, and for I, $\mu_I \approx 22.2 \text{ mag arcsec}^{-2}$. All optical surface brightnesses throughout have units of Vega mag arcsec^{−2}. The surface brightness in the ecliptic plane is roughly 1 mag arcsec^{−2} brighter, $\mu_V \approx 22.35 \text{ mag arcsec}^{-2}$ for ecliptic longitude $\lambda \approx 110^\circ$ –140° and ecliptic latitude $\beta = 0^\circ$ (Table 6.2 in the WFPC2 Handbook; Biretta *et al.* 2000). For KBOs with a Kron-Cousins color of the Sun, V–R = 0.37 mag (Jewitt & Luu 1998; Davies *et al.* 2000), the limit to the R-band surface brightness from KBOs in the ecliptic plane is $\mu_R = 22 \text{ mag arcsec}^{-2}$. Using equation (1), faint KBOs reach this limit at $R \approx 45$ –55 mag (see below). Thus, the KBO number counts cannot follow equation (1) to arbitrarily faint magnitudes.

The far-infrared (far-IR) background radiation place additional constraints on the KBO population. Studies of the collisional evolution of KBOs (e.g., Backman, Dasgupta, & Stencel 1995; Teplitz *et al.* 1999) show that the size dis-

¹We use number counts throughout. The luminosity function, defined as the number per unit volume per magnitude, is more common in extragalactic astronomy. In the Kuiper Belt, the analog to the luminosity function may vary with distance from the Sun.

tribution of objects with radii of several microns to several millimeters should have a power law index $a \approx 3.5$. For small Kuiper Belt grains with temperatures $T_{KBO} \sim 40$ K and a total mass in small grains of $\sim 10^{-5} M_{\oplus}$, far-IR fluxes predicted from these models typically fall below reliably available background measurements at wavelengths longer than $\sim 10 \mu\text{m}$, $I_{\nu}(\text{FIR}) \lesssim 1\text{--}2 \times 10^6 \text{ Jy sr}^{-1}$ (Fixsen *et al.* 1998; Hauser *et al.* 1998). For grains with $T_{KBO} \lesssim 100$ K, we show below that this limit provides a better constraint on the properties of small KBO grains than current surface brightness limits set by *HST*. However, with 1σ sensitivity limits of $\mu_V \approx 27 \text{ mag arcsec}^{-2}$ and $\mu_I \approx 25.4 \text{ mag arcsec}^{-2}$, WFC2 images can, in principle, detect a Kuiper Belt small grain population which emits less light than the currently available far-IR limits.

Our goal is to quantify the relationship between the optical number counts for bright KBOs and the measured sky-surface brightness at optical and far-IR wavelengths. In §2, we use equation (1) to relate the observed sky-surface brightness to the slope of the optical counts. In §3, we derive a physical model relating observables to the KBO size distribution. We conclude in §4.

2. THE OPTICAL SURFACE BRIGHTNESS OF KBOs

For equation (1), the R-band surface brightness for KBOs with magnitude brighter than R is:

$$\mu_R = 41.03 - 2.5 \log \left(\frac{\alpha}{\alpha - 0.4} \right) + (1 - 2.5\alpha) (R - R_0) \quad (2)$$

for $\alpha > 0.4$. The surface brightness at other optical and near-IR bands follows from assumptions for ω and the typical color of a KBO. To relate limits on thermal emission to the optical sky brightness, we assume that F_{tot} is the total flux density in $\text{erg cm}^{-2} \text{ s}^{-1} \text{ sr}^{-1}$ received at Earth from KBOs. If the albedo for KBOs is independent of size, then the R-band surface brightness in mag arcsec^{-2} is:

$$\mu_R = -2.5 \log \left(\frac{\omega F_{tot}}{A_0 F_0} \right) - BC(R), \quad (3)$$

where A_0 is the number of arcsec^2 in a steradian, $F_0 = 2.48 \times 10^{-5} \text{ erg cm}^{-2} \text{ s}^{-1}$ is the zero point (Allen 1976), and $BC(R) = +0.17$ is the bolometric correction (Kenyon & Hartmann 1995). The thermal radiation received from KBOs is $(1 - \omega)F_{tot}$. If KBOs radiate as blackbodies, an absolute upper limit to the flux at frequency ν is the flux at the Planck peak, $I_{\nu,m} \approx 10^{-11} T_{KBO}^{-1} (1 - \omega)F_{tot}$, where T_{KBO} is measured in Kelvins. If we solve equation (3) for F_{tot} , the thermal emission from KBOs depends only on the albedo, the surface brightness, and the temperature:

$$I_{\nu}(\text{FIR}) = 9.5 \times 10^{17-0.4\mu_R} T_{KBO}^{-1} \left(\frac{1 - \omega}{\omega} \right) \text{ Jy sr}^{-1}. \quad (4)$$

For a fixed optical brightness, equation (4) predicts that hot KBOs produce less thermal emission than cold KBOs. This counter-intuitive result is correct, because hot KBOs must have a smaller surface area to emit the same bolometric flux as cold KBOs.

Equation (4) has three main uncertainties. From the apparent spread in the optical colors of KBOs (Jewitt &

Luu 1998; Davies *et al.* 2000), the bolometric correction is uncertain by $\pm 0.2 \text{ mag}$. Large KBOs and comets with $\omega \approx 0.04$ (e.g., Luu & Jewitt 1998) contribute little to the optical surface brightness or the thermal emission. If $\omega \sim 0.2\text{--}0.5$ for the smallest KBO grains (Backman & Paresce 1993; Backman *et al.* 1995), $I_{\nu}(\text{FIR})$ is uncertain by a factor of 4. Small KBO grains with $r \lesssim 100 \mu\text{m}$ are inefficient radiators and are hotter than larger KBOs at the same distance from the Sun (see Backman *et al.* 1995; Teplitz *et al.* 1999). For constant F_{tot} , $I_{\nu}(\text{FIR})$ for small grains is a factor of 2–5 less than the limit in equation (4). We conclude that equation (4) with $\omega = 0.5$ and $T_{KBO} = 40$ K is a reasonable estimate for thermal emission from KBOs with optical number counts defined by equation (1).

The solid lines in Figure 1 indicate how the optical and far-IR surface brightness increase with fainter KBO R-band magnitude, assuming $R_0 = 23.25 \text{ mag}$ and $\alpha = 0.5, 0.6$, and 0.7 . The dashed lines in each panel show observed limits, $I_{\nu}(\text{FIR}) = 10^6 \text{ Jy sr}^{-1}$ and $\mu_R \approx 22 \text{ mag arcsec}^{-2}$. These simple models, which fit the optical counts for $R \leq 26\text{--}27 \text{ mag}$, yield optical and far-IR backgrounds much larger than current limits. The vertical tic marks in Figure 1 indicate approximate radii corresponding to selected R magnitudes for KBOs at 40 AU. The limits on optical and far-IR surface brightness require that the size distribution of KBOs turns over for objects with $r \lesssim 10 \text{ m}$.

To allow for a shallower size distribution of small KBOs, we consider the surface brightness distribution for number counts that follow a broken power law:

$$\log N(R) = \begin{cases} \alpha_1(R - R_0) & R < R_1 \\ \alpha_1(R_1 - R_0) + \alpha_2(R - R_1) & R \geq R_1 \end{cases} \quad (5)$$

Similar forms for broken power laws have been derived for other solar system bodies from observations (e.g., Weissman 1982; Bailey & Stagg 1988) and theory (e.g., Greenberg *et al.* 1984; Wetherill & Stewart 1993). Weissman & Levison (1997) previously proposed a broken power law for KBOs to satisfy constraints from the optical counts and the supply of short period comets.

To construct surface brightness distributions for a broken power law, we adopt $\alpha_1 = 0.6$ and $R_0 = 23.25 \text{ mag}$ to match the optical number counts. Observations currently require $R_1 \geq 26\text{--}27 \text{ mag}$ to fit equation (1) to the optical data. We adopt $R_1 = 30 \text{ mag}$ for simplicity. The dashed lines in Figure 1 show how this model compares with the observed limits for $\alpha_2 = 0.4\text{--}0.5$. Models with $\alpha_2 \lesssim 0.48$ satisfy the optical and far-IR sky-background constraints. The allowed power law slope becomes flatter as the knee in the number counts moves to fainter magnitudes.

3. PHYSICAL MODEL FOR SURFACE BRIGHTNESS

To understand how the constraints on the optical counts relate to the size distribution of KBOs, we construct a physical model for the observed surface brightness. We adopt a broken power law size distribution:

$$n(r) = \begin{cases} n_0(r/r_0)^{-a_1} & r > r_0 \\ n_0(r/r_0)^{-a_2} & r \leq r_0 \end{cases} \quad (6)$$

and assume objects are distributed in a ring around the Sun with a surface density, $\Sigma \propto A^{-\beta}$. The ring has an inner radius $A_1 = 40$ AU and an assumed outer radius $A_2 = 50$ AU. We adjust n_0 and a_1 to match the observed optical counts, $\alpha = 0.6$ and $R_0 = 23.25$ mag, for an adopted $\omega = 0.04$ and slope parameter $g = 0.15$ in the standard two-parameter magnitude relation for sunlight scattered by asteroids (Bowell *et al.* 1989). The slope parameter g relates the brightness of an asteroid at any solar phase angle θ to the brightness at opposition, when $\theta = 0^\circ$. We assume $\theta = 0^\circ$ for these calculations. The predicted μ_R follows from a sum over all objects projected into a box with an area of 1 arcsec^2 . To predict thermal emission from these objects, we use equations (4) and (5) of Backman & Paresce (1993) to derive grain temperatures as a function of distance from the Sun. Large objects absorb and radiate as blackbodies with $T_{KBO} = 278 (1 - \omega)^{1/4} (A/1 \text{ AU})^{-1/2}$; small grains radiate with an emissivity $\epsilon \propto \lambda^{-1}$ and have $T_{KBO} = 468 (1 - \omega)^{1/4} (A/1 \text{ AU})^{-2/5} r^{-1/5}$ where r is the radius in microns (see also Teplitz *et al.* 1999). The thermal emission $I_\nu(\text{FIR})$ follows from the appropriate sum over all bodies in a solid angle of 1 steradian.

This model ignores the complex orbital distribution of KBOs at 35–50 AU, where the bright end of the optical number counts is directly measured. Properties of KBOs beyond 50 AU are unknown. The relationship between μ_R and $I_\nu(\text{FIR})$ is independent of our approximations and uncertainties. Our results are insensitive to β , because we fit the observed optical counts. The model predicts smaller far-IR fluxes for grains with an emissivity $\epsilon \propto \lambda^{-2}$; current observations cannot distinguish between possible emissivity laws. Although specific predictions for the optical and far-infrared surface brightness are sensitive to other adopted parameters, our main conclusions are independent of these assumptions except as indicated below.

The curves in Figure 2 show how the optical and $100 \mu\text{m}$ surface brightness increase with fainter KBO R-band magnitude for models with $\beta = 1.5$, $a_1 = 4$, and $a_2 = 3.0, 3.25$, and 3.5 . Solid lines show results when all objects have $\omega = 0.04$; dot-dashed lines show how the surface brightness changes when the albedo varies smoothly from $\omega = 0.04$ for $r \geq 1 \text{ km}$ to $\omega = 0.5$ for $r \leq 0.1 \text{ km}$. As expected, the larger albedo produces a brighter optical surface brightness, but a fainter far-IR surface brightness. For models with $a_2 = 3.5$, KBOs with a small constant albedo have a limiting optical surface brightness, $\sim 24.5 \text{ mag arcsec}^{-2}$, fainter than the observed sky brightness. This limit, however, is detectable with *HST* if other background sources can be reliably subtracted. If small KBOs have $a_2 = 3.5$ and a large albedo, the predicted μ_R exceeds the observed background at $R \sim 70$ mag. This limit corresponds to objects with $r \sim 0.03 \text{ mm}$. In both cases, the far-IR surface brightness exceeds the measured sky brightness for $\lambda \leq 240 \mu\text{m}$ at $R \approx 65\text{--}70$ mag. The predicted far-IR surface brightness lies below measured limits at longer wavelengths.

The far-IR surface brightness at $100 \mu\text{m}$ flattens in Figure 2 for $R \geq 70$ mag, because grains with $r \lesssim 100 \mu\text{m}$ radiate inefficiently and are too hot to emit much $100 \mu\text{m}$ light. If the albedo of these small grains remains large, constraints on the KBO small grain population from optical data are stronger than the COBE constraints for $R \lesssim 75$ mag (i.e., $r \leq 1\text{--}3 \mu\text{m}$). Uncertain optical properties

for small KBO grains and rapid grain removal processes such as Poynting-Robertson drag make it difficult to use any observation to constrain the mass in KBO grains with $R \gtrsim 75$ mag.

The results in Figure 2 show that the predicted surface brightness is very sensitive to a_2 , the power law slope of the small object size distribution. Models with $a_2 \leq 3.4$ are consistent with the surface brightness limits set by *COBE* for $\lambda \geq 10 \mu\text{m}$ and by *HST* at V and I. Models with $a_2 \leq 3.25$ predict background fluxes well below current detection limits at all wavelengths.

4. DISCUSSION AND SUMMARY

Our results demonstrate a clear relationship between the optical and far-IR surface brightness from KBOs in the outer solar system. The relation depends only on ω and T_{KBO} . Direct measurements of μ_R and I_ν from KBOs should yield direct constraints on ω and T_{KBO} for small grains. Observations of μ at other optical and near-IR wavelengths measure the colors of small KBOs.

The optical and far-IR surface brightness place useful constraints on the size distribution of small KBOs. To avoid violating Olbers Paradox at optical and far-IR wavelengths, the slope of the optical counts must change from $\alpha_1 \approx 0.6$ at $R \lesssim 27$ mag to $\alpha_2 \lesssim 0.48$ at $30 \leq R \leq 50$ mag. With $a = 5\alpha + 1$, the slope of the KBO size distribution must change from $a_1 \approx 4$ for $r \gtrsim 10 \text{ km}$ to $a_2 \lesssim 3.4$ for $1 \text{ m} \leq r \leq 1 \text{ km}$. This conclusion is independent of assumptions about ω , T_{KBO} , or the space distribution of KBOs. If many small KBOs lie beyond 50 AU, the knee in the size distribution must occur at $r \gtrsim 1 \text{ m}$.

Our upper limit for α_2 is larger than the usual result for Olbers paradox, $\alpha_2 \leq 0.4$. In extragalactic astronomy, galaxies fill an infinite volume nearly uniformly; galaxy counts with $\alpha \geq 0.4$ always produce a divergent sky brightness. For dust grains, the sky brightness converges when the largest objects produce all of the light ($a \leq 3$, $\alpha \leq 0.4$); the sky brightness diverges when the smallest objects produce all of the light ($a > 3$, $\alpha > 0.4$). Because dust grains and the disk of our solar system have finite sizes, the sky brightness can converge for $\alpha > 0.4$. For grains with $r \gtrsim 0.01 \mu\text{m}$ at 40–50 AU, models with $\alpha_2 \leq 0.47$ do not violate Olbers Paradox. If Poynting-Robertson drag and radiation pressure are effective at removing grains with $r \leq 1 \mu\text{m}$, this limit is raised to $\alpha_2 \leq 0.48$.

These results support coagulation models for the formation of the Kuiper Belt during the early evolution of our solar system (Kenyon & Luu 1999a,b). In this picture, small objects with $r \lesssim 1\text{--}100 \text{ m}$ collide and merge to form larger objects. In 10–100 million years, coagulation leads to a population of 1–1000 km objects with a size distribution $n(r) \propto r^{-4}$. Smaller objects have a shallower size distribution, $n(r) \propto r^{-3.5}$ (Kenyon & Luu 1999a; Backman *et al.* 1995). Orbital evolution of KBOs leads to large collisional velocities and gradual erosion of the Kuiper Belt (Holman & Wisdom 1993). Collisions between high velocity objects produce debris which adds to the ‘collisional tail’ where $n(r) \propto r^{-3.5}$ (Davis & Farinella 1997). Poynting-Robertson drag and radiation pressure remove objects with radii less than 1 mm on timescales roughly proportional to the grain radius, $\sim 10^6 \text{ yr } (r/1 \mu\text{m})$ (Burns *et al.* 1979; Backman & Paresce 1993). Grain removal may lead to a size distribution slightly flatter than

$n(r) \propto r^{-3.5}$ for $r \sim 1 \mu\text{m}$ to 1 mm at $35\text{--}50 \text{ AU}^2$. Our analysis, together with those of previous investigations, demonstrates that the transition from a merger population with $n(r) \propto r^{-4}$ to a debris population with $n(r) \propto r^{-3.4}$ must occur at radii $10\text{--}1000 \text{ m}$, where collisions should produce debris instead of mergers.

If other background sources can be reliably subtracted, current and future space missions can detect the integrated scattered light and thermal emission from small KBOs. Direct detection of KBOs in the optical/near-IR or far-IR background would begin to provide stringent tests of collision models. Constraints on the variation of surface brightness with ecliptic latitude or longitude would allow direct measurements of the scale height and orbital distributions of small KBOs. In addition to possible ground-

based strategies, the sensitivity of deep HST WFPC2 images is now sufficient to improve constraints on the KBO optical background by a factor of ten. The *Space Infrared Telescope Facility* can improve the far-IR constraints by a similar factor. The *Next Generation Space Telescope* will provide direct measurements of individual KBOs near the proposed knee in the size distribution at $R \approx 28\text{--}31 \text{ mag}$ and more accurate background measurements in the optical and near-IR. These and other facilities will yield better understanding of the implications of Olbers Paradox in our solar system and beyond.

Comments from M. Geller, M. Holman, B. Marsden, and an anonymous referee improved the accuracy and quality of the manuscript.

REFERENCES

- Ilen, C. W. 1976, *Astrophysical Quantities*, Athlone, London, p. 197
- Backman, D. E., Dasgupta, A., & Stencel, R. E. 1995, ApJ, 450, L35
- Backman, D. E., & Paresce, F. 1993, in *Protostars and Planets III*, eds. E. H. Levy & J. I. Lunine, Tucson, Univ of Arizona, p. 1253
- Bailey, M. A., & Stagg, C. R. 1988, MNRAS, 235, 1
- Biretta *et al.* 2000, WFPC2 Instrument Handbook, Version 5.0 (Baltimore: STScI)
- Bowell, E., Hapke, B., Domingue, D., Lumme, K., Peltoniemi, J., and Harris, A. W. 1989, in *Asteroids II*, eds. R. P. Binzel, T. Gehrels, & M. S. Matthews, Tucson, Univ. of Arizona Press, p. 524.
- Burns, J. A., Lamy, P. L., & Soter, S. 1979, Icarus, 40, 1
- Chiang, E. I., & Brown, M. E. 1999, AJ, 118, 1411
- Davies, J. K., Green, S., McBride, N., Muzzerall, E., Tholen, D. J., Whiteley, R. J., Foster, M. J., & Hillier, J. K. 2000, Icarus, 146, 253
- Davis, D. R., & Farinella, P. 1997, Icarus, 125, 50
- Driver, S. P., Windhorst, R. A., Ostrander, E. J., Keel, W. C., Griffiths, R. E., & Ratnatunga, K. U. 1995, ApJ, 449, L023
- Driver, S. P., Windhorst, R. A., Philipps, S., & Bristow, P. D. 1996, ApJ, 461, 525
- Driver, S. P., Fernandez-Soto, A., Couch, W. J., Odewahn, S. C., Windhorst, R. A., Philipps, S., Lanzetta, K., & Yahil, A. 1998, ApJ, 496, L093
- Fixsen, D. J., Dwek, E., Mather, J. C., Bennett, C. L. & Shafer, R. A. 1998, ApJ, 508, 123
- Gladman, B., Kavelaars, J. J., Nicholson, P. D., Lored, T. J., & Burns, J. A. 1998, AJ, 116, 2042
- Greenberg, R., Weidenschilling, S. J., Chapman, C. R., & Davis, D. R. 1984, Icarus, 59, 87
- Hauser, M. G. *et al.* 1998, ApJ, 508, 25
- Holman, M. J., & Wisdom, J. 1993, AJ, 105, 1987
- Jewitt, D., Luu, J., & Chen, J. 1996, AJ, 112, 1225
- Jewitt, D., & Luu, J. X. 1998, AJ, 115, 1667
- Jewitt, D., Luu, J. X., & Trujillo, C. 1998, AJ, 115, 2125
- Kenyon, S. J., & Hartmann, L. 1995, ApJS, 101, 117
- Kenyon, S. J., & Luu, J. X. 1999, AJ, 118, 1101
- Kenyon, S. J., & Luu, J. X. 1999, ApJ, 526, 465
- Luu, J. X., & Jewitt, D. 1998, ApJ, 502, L91
- Luu, J. X., Marsden, B., Jewitt, D., Trujillo, C. A., Hergenrother, C. W., Chen, J., & Offutt, W. B. 1997, Nature, 387, 573
- Odewahn, S. C., Windhorst, R. A., Driver, S. P., & Keel, W. C. 1996, ApJ, 472, L013
- Teplitz, V. I., Stern, S. A., Anderson, J. D., Rosenbaum, D., Scalise, R. I., & Wentzler, P. 1999, ApJ, 516, 425
- Trujillo, C. A., Jewitt, D. C., & Luu, J. X. 2000, ApJ, 529, L103
- Weissman, P. R. 1982, in *Geological Implications of Impacts of Large Asteroids and Comets on the Earth*, eds. L. T. Silver & P. H. Schultz, GSA SP-190, Boulder, Geological Soc. of America, p. 15
- Weissman, P. R., & Levison, H. F. 1997, in *Pluto and Charon*, eds. S. A. Stern, D. J. Tholen, & A. R. Schumer, Tucson, Univ of Arizona Press, p. 559
- Wetherill, G. W., & Stewart, G. R. 1993, Icarus, 106, 190
- Windhorst, R., Mathis, D. F., & Keel, W. C. 1992, ApJ, 400, L1
- Windhorst, R. A., Gordon, J. M., Pascarelle, S. M., Schmidtke, P. C., Keel, W. C., Burkey, J. M., & Dunlop, J. S. 1994, ApJ, 435, 577
- Windhorst, R. A., Keel, W. C., & Pascarelle, S. M. 1998, ApJ, 494, L27

²In the inner solar system at $1\text{--}2 \text{ AU}$, Poynting-Robertson drag and radiation pressure timescales are ~ 1000 times shorter than in the Kuiper Belt, which leads to rapid removal of grains with radii of 1 mm or smaller. Very small grains in the inner solar system thus make a negligible contribution to the brightness of the night sky.

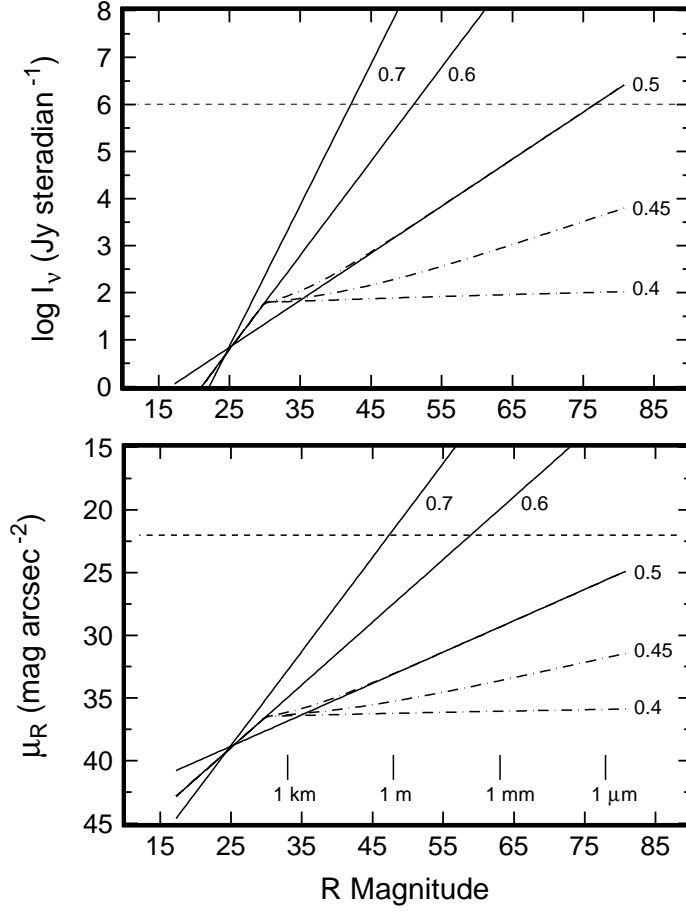


FIG. 1.— Far-infrared and optical surface brightness as a function of R magnitude. Each panel shows how the integrated surface brightness increases with the R-magnitude limit for models with a single power law for the number counts (solid curves; equations 1, 2, and 4) or a broken power law fit to the number counts (dot-dashed curves; equation 5). Values for the power law slope, α , appear to the right of each solid curve. Dot-dashed curves have $\alpha_1 = 0.6$ and α_2 as indicated. Each model is consistent with observations of the optical counts at $R \leq 26\text{--}27$.

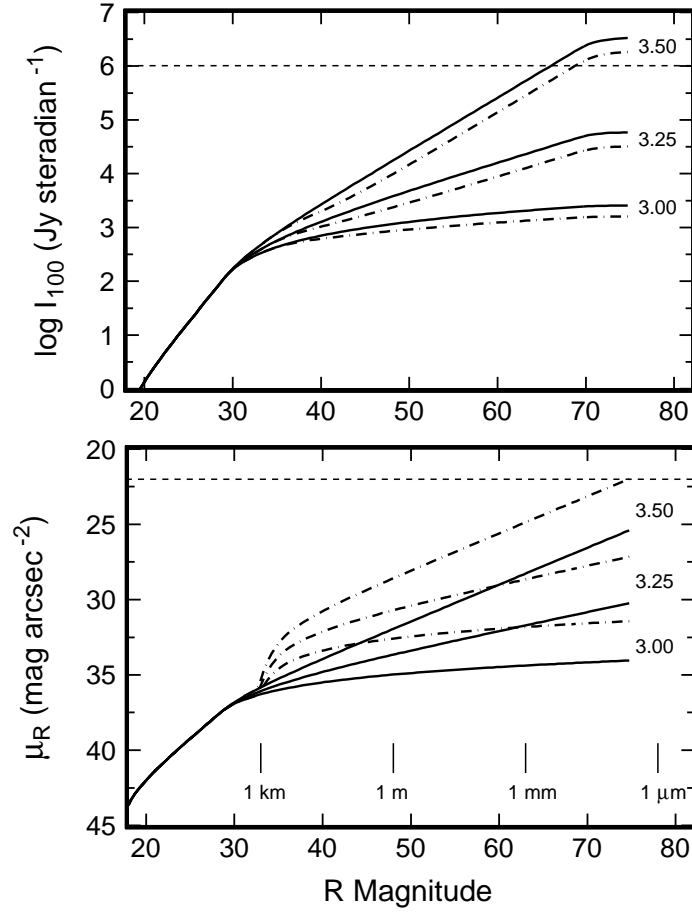


FIG. 2.— As in Figure 1 for a physical KBO model. The model assumes a broken power law size distribution, equation (6), albedo ω , and a surface density distribution for KBOs in a ring at 40–50 AU. Solid curves show results for $a_1 = 4$, $\omega = 0.04$, and a_2 as indicated at the right end of each curve. Dot-dashed curves repeat this model for small grains with larger ω as described in the text. Each model is consistent with observations of the optical counts at $R \leq 26$ –27.